Lattice thermal conductance in nanowires at low temperatures: Breakdown and recovery of quantization

Y. Tanaka,[1,2] F. Yoshida,[1] and S. Tamura[1]
[1]*Department of Applied Physics, Hokkaido University, Sapporo 060-8628, Japan*
[2]*Department of Physics and Astronomy, Dartmouth College, Hanover, New Hampshire 03755, USA*
(Received 27 December 2004; published 20 May 2005)

The quantization of lattice thermal conductance g normalized by $g_0=\pi^2k_B^2T/3h$ (the universal quantum of thermal conductance) was recently predicted theoretically to take an integer value over a finite range of temperature and then observed experimentally in nanowires with catenoidal contacts. The prediction of this quantization by Rego and Kirczenow [Phys. Rev. Lett. **81**, 232 (1998)] relies on a study of only dilatational (longitudinal) vibrational mode in the wires. We study the thermal conductance in catenoidal wires by explicitly calculating the transmission rates of the six distinct vibrational modes (four acoustic and two low-lying optical modes) and applying the Landauer formula for the one-dimensional thermal transport in the ballistic regime. In a temperature range similar to the one predicted by Rego and Kirczenow, we find the presence of a plateau in g/g_0. However, below this temperature range g/g_0 is modified—that is, the quantization is broken—due to imperfect transmission of the acoustic modes of vibration. Our new observation is that, as temperature goes down further, the recovery of the quantization of g/g_0 should occur. These results are found assuming GaAs as a wire material, but we also make similar calculations for silicon nitride wires used experimentally.

DOI: 10.1103/PhysRevB.71.205308 PACS number(s): 65.80.+n, 61.46.+w, 62.30.+d, 63.22.+m

I. INTRODUCTION

Fabrication of suspended nanoscale structures has allowed various new observations related to the quantum nature of the thermal transport and mechanical vibrations.[1,2] In particular, the experimental observation of the quantized thermal conductance in dielectric nanowires of catenoidal shape has recently been reported;[3,4] that is, the lattice thermal conductance becomes an integer multiple of $g_0=\pi^2k_B^2T/3h=(9.465\times10^{-13}\ \mathrm{W\,K^{-2}})\ T$, the universal thermal conductance quantum. This quantization has theoretically been predicted in a ballistic phonon regime by applying the Landauer formula originally used for the electrical conductance.[5–7] A tacit assumption for this quantization is that the transmission of heat, or thermal phonons, in a nanowire is perfect. However, the transmission characteristics of phonons through the nanowires crucially depends on both their shapes and contacts between the wire and heat reservoirs (the heat source and sink), even if the scatterings of phonons inside the wires are neglected. In addition, the transmission rate depends on the frequency and mode of phonons, or lattice vibrations.

Through their analysis of the thermal conductance for various contact shapes, Rego and Kirczenow[5] found that a distinct plateau develops for g/g_0 over a wide range of temperatures if a catenoidal wire with cross-sectional area varying as

$$A(x)=A_0\cosh^2(x/\lambda) \tag{1}$$

(with A_0 a constant) is assumed. More explicitly, they considered the wire with a *rectangular* cross-sectional area $A(x)=hl(x)$ with a constant thickness h in the z direction and a varying width $l(x)=h\cosh^2(x/\lambda)$ in the y direction. Here we note that the parameter λ measures the length of the wire over which the cross-sectional area can be regarded to be uniform. Hence, we call 2λ the effective length of the wire. However, their analysis is restricted to the longitudinal (dilatational) vibrational mode only and other acoustic modes which should equally contribute to the thermal conductance have not explicitly been studied. Here we remark that, in a catenoidal wire, the lowest four vibrational branches (including the dilatational mode) to be studied have cutoff frequencies depending on λ. But these cutoffs vanish in the limit of large λ. So we conveniently call those four modes of vibrations acoustic modes.

In the present study, we investigate the transmission characteristics of the six low-lying vibrational modes (four acoustic modes and two lowest optical modes) which play important roles in the thermal transport in catenoidal nanowires at temperatures around 1 K and consider how the resulting thermal conductance g/g_0 changes as the temperatures decrease further. At low frequencies the transmission rate of vibrational modes through the wires shows, in general, complicated behavior including resonances and cutoffs. This means that quantization of thermal conductance relying on perfect phonon transmission should be no longer valid as the temperature goes down to 0 K, where only low-frequency vibrations transport heat inside the wires. To convince ourselves of this naive expectation and also to supplement the study of Rego and Kirczenow,[5] we calculate the transmission rates of the lowest four acoustic vibrational modes—that is, the dilatational, torsional, and two types of flexural modes—as well as two shear modes (the optical modes) that are coupled to the flexural modes in the wires. For this purpose we employ the Timoshenko model for vibrations of an elastic beam rather than the simpler Bernoulli-Euler theory.[11,12] Then, either the transfer- or scattering-matrix method is applied to the numerical evaluation of the transmission rates in the wires with varying cross-sectional area. The resulting transmission rates are incorporated into the Landauer formula for the thermal conductance ratio g/g_0

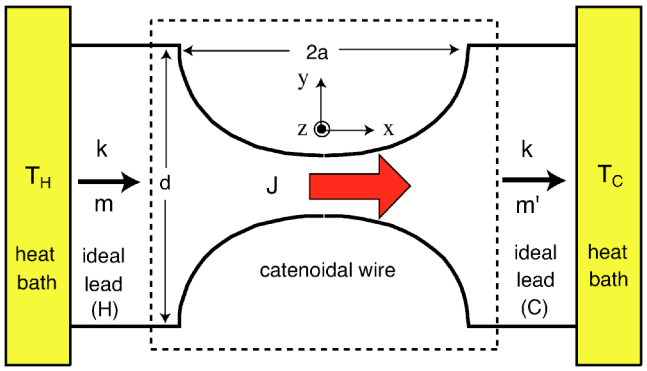

FIG. 1. Diagram defining the heat flow J in the system consisting of a catenoidal wire (thickness h in z direction is uniform). The wire is attached to the ideal leads (labeled H and C) in which the wave number k and vibrational modes m and m' are defined. The ideal leads are also attached to the hot and cold heat reservoirs with temperatures T_H and T_C, respectively.

and we study its temperature dependence from the previously reported plateau region (1–0.1 K) (Refs. 3–5) down to the sub-mK region. While our calculations are developed mainly for GaAs wires in order to compare with the theory of Rego and Kirczenow, we also consider them for silicon nitride wires with parameters relevant for the experiments by Schwab *et al.*[3,4]

In the next section, after briefly reviewing the theory of the lattice thermal conductance, we formulate the equations of motion for the lowest six vibrational modes in a catenoidal wire. The transmission rates of these vibrational modes through the catenoidal wire are then studied in Sec. III based on the transfer-matrix method (and also the scattering-matrix method). We present numerical results for typical wire parameters as well as analytical results for the dilatational mode. With these results for the transmission rates, the calculation of the thermal conductance is presented in Sec. IV. In Sec. V, the characteristic behavior of the thermal conductance obtained is discussed in terms of the various length scales characterizing the catenoidal wire. Conclusions are given in Sec. VI. In Appendix A, we give explicit expressions for the basic matrices needed for the transfer-matrix formalism of each mode. The scattering-matrix formalism for the transmission rates is given in Appendix B.

II. THERMAL CONDUCTANCE AND VIBRATIONAL EQUATIONS OF MOTION

The Landauer formula[8,9] applied to the heat current J in a one-dimensional dielectric wire suspended between hot and cold heat reservoirs of temperatures T_H and T_C (Fig. 1) is[5,6]

$$J = \sum_m \int_0^\infty \frac{dk}{2\pi} \hbar \omega_m(k) V_m(k) [n_{H,m} - n_{C,m}] |t_m(k)|^2, \quad (2)$$

where m denotes vibrational modes in the wire, k is the wave number along the wire defined in the ideal leads attached to the wire, ω_m is the angular frequency, V_m is the group velocity, $n_{H,m}(n_{C,m})$ is the Planck distribution for the hot (cold) reservoir, and $|t_m|^2$ is the transmission rate through the wire. Phonon scatterings are assumed to occur only between the ideal leads and the wire and their effects are included in the transmission coefficient t_m. The scatterings happening inside or at the surface of the wire[10] are not considered. Here we note that some of the vibrational modes in the wire are coupled to each other and the mode conversion occurs while they are transmitted through the wire. Thus the sum over the transmitted modes (m' in Fig. 1) is also necessary but this can be included in the definition of the transmission rate $|t_m|^2$ (see Sec. III).

The thermal conductance g is given by $g = J/\delta T$ in the limit $\delta T = T_H - T_C \to 0$. Hence, at $T = (T_H + T_C)/2$ we have

$$g = \frac{1}{2\pi} \sum_m \int_{\tilde{\omega}_m}^\infty d\omega \, \hbar\omega \frac{\partial n(\omega, T)}{\partial T} |t_m(\omega)|^2$$
$$= \frac{k_B^2 T}{h} \sum_m \int_{x_m}^\infty dx \frac{x^2 e^x}{(e^x - 1)^2} \left| t_m\left(\frac{k_B T}{\hbar} x\right) \right|^2, \quad (3)$$

where $\tilde{\omega}_m$ is the minimum frequency of the mode m and $x_m = \hbar\tilde{\omega}_m / k_B T$. If we can put $|t_m|^2 = 1$ and $x_m = 0$ in Eq. (3), we have $g = N_{ac} g_0$. Note that $x_m = 0$ means that only massless acoustic branches (N_{ac} is their number) contribute to the thermal transport.

Although the vibrational equations of motion for the wires with a uniform cross-sectional area are readily solved, these wires do not necessarily work as good waveguides for heat when the contacts with heat reservoirs (through leads) are taken into account. As shown by Rego and Kirczenow,[5] an adiabatic contact between the thermal reservoirs and the ballistic quantum wire of a catenoidal shape [with the cross-sectional area changing according to Eq. (1)] gives a better transmission characteristic for heat transport. Unfortunately, however, Rego and Kirczenow analyzed only the dilatational mode of vibration and they expected that the results applied to other acoustic modes as well.

We now explicitly study the transmission characteristic of the six low-lying vibrational modes in a catenoidal nanowire, which should contribute to the thermal transport at temperatures around 1 K and less.

A. Dilatational mode

The equation of motion for dilatational (longitudinal) vibrations in a wire (extending in the x direction) with a variable cross-sectional area $A(x)$ is

$$\rho A(x) \frac{\partial^2 u}{\partial t^2} = \frac{\partial}{\partial x} \left[A(x) Y \frac{\partial u}{\partial x} \right], \quad (4)$$

where ρ is the mass density and $Y \partial u / \partial x = \sigma$ is the stress with Y the Young modulus of the wire material (assumed isotropic elastically). For a wire with a uniform cross section, this equation is reduced to a simple wave equation in one dimension:

$$\frac{1}{v_l^2}\frac{\partial^2 u}{\partial t^2} = \frac{\partial^2 u}{\partial x^2}, \tag{5}$$

where $v_l = (Y/\rho)^{1/2}$ is the longitudinal sound velocity. However, for a catenoidal wire characterized by Eq. (1), Eq. (4) is written as

$$\frac{1}{v_l^2}\frac{\partial^2 u}{\partial t^2} = \frac{2}{\lambda}\tanh\left(\frac{x}{\lambda}\right)\frac{\partial u}{\partial x} + \frac{\partial^2 u}{\partial x^2}. \tag{6}$$

This equation is known to have an outgoing-wave solution[13]

$$u = u_0 \cosh^{-1}\left(\frac{x}{\lambda}\right)\exp[i(kx - \omega t)], \tag{7}$$

where u_0 is a constant and the wave number k and frequency ω should satisfy the dispersion relation

$$\omega^2 = v_l^2\left[k^2 + \left(\frac{1}{\lambda}\right)^2\right]. \tag{8}$$

Thus, a cutoff frequency $\omega_D^c \equiv v_l/\lambda$ exists for this mode (although it vanishes for $\lambda \to \infty$). For $\omega < \omega_D^c$ the wave number k is pure imaginary and the vibrations do not propagate through the wire.

B. Torsional mode

The equation of motion for the torsional mode is

$$\rho\tilde{I}(x)\frac{\partial^2\theta}{\partial t^2} = \frac{\partial}{\partial x}\left[C(x)\frac{\partial\theta}{\partial x}\right], \tag{9}$$

where θ is the angle of twist of the wire, $\tilde{I}(x) = \int(y^2+z^2)dA$ is the polar moment of inertia, and $C(x)\partial\theta/\partial x = \tau(x)$ is the torque with $C(x)$ the torsional rigidity depending on the shear modulus G of the wire and on the cross-sectional properties. If the wire has a uniform cross section [$C(x) = C_0$ and $\tilde{I}(x) = \tilde{I}_0$, with C_0 and $\tilde{I}_0$ constants], this equation of motion again becomes a wave equation

$$\frac{\partial^2\theta}{\partial t^2} = \frac{C_0}{\rho\tilde{I}_0}\frac{\partial^2\theta}{\partial x^2}, \tag{10}$$

and the dispersion relation is given by $\omega = (C_0/\rho\tilde{I}_0)^{1/2}k$.

For a wire with a rectangular cross-sectional area $A(x) = hl(x)$, we have

$$\tilde{I}(x) = \frac{1}{12}[h^3 l(x) + h l^3(x)] \tag{11}$$

and the torsional rigidity is given by Timoshenko and Goodier as[11]

$$C(x) = G\frac{h^3 l(x)}{3}\left\{1 - \frac{192h}{\pi^5 l(x)}\sum_{m=1,3,5,\ldots}^{\infty}\frac{1}{m^5}\tanh\left[\frac{m\pi l(x)}{h}\right]\right\}. \tag{12}$$

For the catenoidal wire we will consider—i.e., $l(x) = h\cosh^2(x/\lambda)$—this expression (12) is well approximated to be

$$C(x) = \frac{Gh^3}{3}[l(x) - 0.627h] \tag{13}$$

and Eq. (9) is reduced to

$$\frac{\partial^2\theta}{\partial x^2} + \frac{l'(x)}{l(x) - 0.627h}\frac{\partial\theta}{\partial x} = \frac{h^2 l(x) + l^3(x)}{4h^2[l(x) - 0.627h]}\frac{1}{v_t^2}\frac{\partial^2\theta}{\partial t^2}, \tag{14}$$

where $v_t = (G/\rho)^{1/2}$ is the transverse sound velocity. Unfortunately, this equation of motion cannot be solved analytically.

If we consider the region $x \gg \lambda$ (near the end of the wire), $l(x) = h\cosh^2(x/\lambda) \gg h$ and Eq. (14) is approximated as

$$\frac{\partial^2\theta}{\partial x^2} + \frac{2}{\lambda}\frac{\partial\theta}{\partial x} + \frac{\cosh^4(x/\lambda)}{4}\left(\frac{\omega}{v_t}\right)^2\theta = 0, \tag{15}$$

where we have put $\theta \propto \exp(-i\omega t)$. [For $x \ll -\lambda$, λ should be replaced by $-\lambda$ in Eq. (15).] Let us subdivide the wire into small segments in the x direction and regard the cross-sectional area as uniform in each segment—i.e., $\cosh^2(x/\lambda) = \cosh^2(x_n/\lambda)$ with x_n the position of the nth segment (this division will be used in Sec. III for the calculation of transmission rates). Then, Eq. (15) has a solution $\theta \propto \exp[i(kx - \omega t)]$, where

$$k = \pm\left[\frac{\cosh^4(x_n/\lambda)}{4}\left(\frac{\omega}{v_t}\right)^2 - \left(\frac{1}{\lambda}\right)^2\right]^{1/2} + \frac{i}{\lambda}. \tag{16}$$

This equation can be used to estimate the cutoff frequency ω_T^c of the torsional mode—i.e., $\omega_T^c \equiv 2v_t/[\lambda\cosh^2(x_n/\lambda)]$ Thus, the cutoff frequency depends on the position of the segment and takes the smallest value at the both ends of the wire. Here we note that Eq. (15) has an extended solution $\theta(x)$ at $\omega = 0$.

C. Transverse modes resulting from bending motions

The Bernoulli-Euler theory applied to the bending motion of a wire leads to the unphysical consequence that the wave velocity increases indefinitely with increasing wave number.[12] As formulated by Timoshenko and Goodier, both the flexural and shear motions associated with the bending of the wire are coupled to each other.[11] The equations of motion describing the coupled flexural and shear motions lead, for a wire with a uniform cross section, to the correct wave velocity obtained by the elasticity theory. For these coupled modes the dynamical variables are the displacement w transverse to the neutral surface of the wire and the angle ψ which measures the slope of the wire cross section relative to the $y(z)$ axis when the displacement w is associated with the bending in the $y(z)$ direction. In the Bernoulli-Euler theory this angle is the same as the slope of the centroidal axis $\partial w/\partial x$. But the shearing effect introduces an additional contribution. The equations of motion governing the displacements w and ψ are

$$\rho A(x)\frac{\partial^2 w}{\partial t^2} = \kappa G\frac{\partial}{\partial x}\left[A(x)\left(\frac{\partial w}{\partial x} - \psi\right)\right], \tag{17}$$

$$\rho I(x)\frac{\partial^2\psi}{\partial t^2} = Y\frac{\partial}{\partial x}\left[I(x)\frac{\partial\psi}{\partial x}\right] + \kappa GA(x)\left(\frac{\partial w}{\partial x} - \psi\right), \quad (18)$$

where κ is the shear coefficient (=0.833 for a rectangular cross section),[11] $A(x)=hl(x)$, and I is the moment of inertia of area defined by $I(x)=\int z^2 dA = h^3 l(x)/12 \equiv I_z(x)$ for the bending in the z (the thickness) direction with z the coordinate to the neutral surface of the wire. Similarly, $I(x)=\int y^2 dA = hl^3(x)/12 \equiv I_y(x)$ for the bending in the y (the width) direction.

For a wire with a uniform cross section (of area A_0) these equations are reduced to

$$\rho\frac{\partial^2 w}{\partial t^2} = \kappa G\left(\frac{\partial^2 w}{\partial x^2} - \frac{\partial\psi}{\partial x}\right), \quad (19)$$

$$\rho I_0\frac{\partial^2\psi}{\partial t^2} = YI_0\frac{\partial^2\psi}{\partial x^2} + \kappa GA_0\left(\frac{\partial w}{\partial x} - \psi\right), \quad (20)$$

where $I(x)$ is also independent of x and we have put $I(x)=I_0$. By putting $w, \psi \sim \exp[i(kx-\omega t)]$, we obtain the equation determining the dispersion relations in this uniform wire as

$$\rho^2 I_0\omega^4 - \rho\omega^2[\kappa GA_0 + (\kappa G + Y)I_0 k^2] + \kappa GYI_0 k^4 = 0. \quad (21)$$

The flexural mode has a frequency ω that vanishes in the long-wavelength limit ($k\to 0$). Explicitly, the dispersion relation of this mode is expressed as $\omega=(YI_0/\rho A_0)^{1/2}k^2$ for $k \simeq 0$. So this is an acoustic branch. In contrast, the shear mode has a finite frequency at $k=0$, which is given by $\omega=\omega_{S,min}\equiv(\kappa GA_0/\rho I_0)^{1/2}$. This cutoff arises from the lateral confinement of the vibration in the wire. Hence, the excitation of the shear mode is related to the onset of three-dimensional heat conduction in a wire. For a large k, Eq. (21) leads to $\omega=(Y/\rho)^{1/2}k=v_l k$ and $\omega=(\kappa G/\rho)^{1/2}k=\kappa^{1/2}v_t k$, for the flexural and shear modes, respectively.

Here we give an approximate equation of motion for the flexural mode valid at low frequencies obtained by neglecting the coupling to the shear mode of vibrations:

$$\rho A(x)\frac{\partial^2 w}{\partial t^2} = -\frac{\partial^2}{\partial x^2}\left[YI(x)\frac{\partial^2 w}{\partial x^2}\right]. \quad (22)$$

For the vibrations in the thickness (z) direction $I(x)=I_z(x)$ and Eq. (22) becomes [by putting $w\propto\exp(-i\omega t)$]

$$\frac{\partial^4 w}{\partial x^4} + \frac{4}{\lambda}\tanh\left(\frac{x}{\lambda}\right)\frac{\partial^3 w}{\partial x^3} + \frac{2}{\lambda^2}\left[1+\tanh^2\left(\frac{x}{\lambda}\right)\right] \times\frac{\partial^2 w}{\partial x^2} - 12\left(\frac{\omega}{v_l h}\right)^2 w = 0, \quad (23)$$

which is reduced to

$$\frac{\partial^4 w}{\partial x^4} + \frac{4}{\lambda}\frac{\partial^3 w}{\partial x^3} + \frac{4}{\lambda^2}\frac{\partial^2 w}{\partial x^2} - 12\left(\frac{\omega}{v_l h}\right)^2 w = 0, \quad (24)$$

for $x \gg \lambda$. (For $x \ll -\lambda$ we may again change λ to $-\lambda$.)

For the vibrations of the catenoidal wire [Eq. (1)] in the width (y) direction $I(x)=I_y(x)$ and Eq. (22) becomes

$$\frac{\partial^4 w}{\partial x^4} + \frac{12}{\lambda}\tanh\left(\frac{x}{\lambda}\right)\frac{\partial^3 w}{\partial x^3} + \frac{6}{\lambda^2}\left[1+5\tanh^2\left(\frac{x}{\lambda}\right)\right] \times\frac{\partial^2 w}{\partial x^2} - \frac{12\omega^2}{v_l^2 h^2\cosh^4(x/\lambda)}w = 0, \quad (25)$$

which is reduced to

$$\frac{\partial^4 w}{\partial x^4} + \frac{12}{\lambda}\frac{\partial^3 w}{\partial x^3} + \frac{36}{\lambda^2}\frac{\partial^2 w}{\partial x^2} - 12\left[\frac{\omega}{v_l h\cosh^2(x/\lambda)}\right]^2 w = 0, \quad (26)$$

for $x \gg \lambda$.

Now, the solution $w=w_z(x)$ of Eq. (24) is

$$w_z(x) = \sum_{j=1}^{4} a_j \exp(\kappa_j^z x), \quad (27)$$

where a_j ($j=1-4$) are arbitrary constants,

$$\kappa_{1,2}^z = -\frac{1}{\lambda} \pm i\left[\frac{2\sqrt{3}\omega}{v_l h} - \left(\frac{1}{\lambda}\right)^2\right]^{1/2} \quad (28)$$

and

$$\kappa_{3,4}^z = -\frac{1}{\lambda} \pm \left[\frac{2\sqrt{3}\omega}{v_l h} + \left(\frac{1}{\lambda}\right)^2\right]^{1/2}. \quad (29)$$

Thus, we estimate that there exists a cutoff frequency for this mode given by $\omega_{F,z}^c = v_l h/2\sqrt{3}\lambda^2$.

Next, we consider the solution of Eq. (26) again in a small segment of the wire (as in Sec. II B for the torsional mode) where $\cosh^2(x/\lambda)$ can be regarded to be constant—i.e., $\cosh^2(x/\lambda)=\cosh^2(x_n/\lambda)$ with x_n the position of the segment. Then the solution $w=w_y(x)$ of Eq. (26) takes the form

$$w_y(x) = \sum_{j=1}^{4} b_j \exp(\kappa_j^y x), \quad (30)$$

where b_j ($j=1-4$) are constants,

$$\kappa_{1,2}^y = -\frac{3}{\lambda} \pm i\left[\frac{2\sqrt{3}\omega}{v_l h\cosh^2(x_n/\lambda)} - \left(\frac{3}{\lambda}\right)^2\right]^{1/2} \quad (31)$$

and

$$\kappa_{3,4}^y = -\frac{3}{\lambda} \pm \left[\frac{2\sqrt{3}\omega}{v_l h\cosh^2(x_n/\lambda)} + \left(\frac{3}{\lambda}\right)^2\right]^{1/2}. \quad (32)$$

Hence, for this mode, the cutoff frequency is estimated to be $\omega_{F,y}^c = 9v_l h\cosh^2(x_n/\lambda)/2\sqrt{3}\lambda^2$ and this becomes largest at both ends of the wire.

III. TRANSMISSION RATE

It is only for the dilatational mode that an analytic solution has been obtained for the above vibrational equations of motion for the catenoidal wire.[13] Thus, for the calculation of the transmission rates we need a numerical scheme. In the present work, we employ the transfer-matrix method for the dilatational and torsional modes (numerically stable) and the

scattering-matrix method[14] for the coupled flexural and shear modes for which the transfer-matrix method becomes numerically unstable at high frequencies. (For the scattering-matrix method, see the Appendix B.) Here, the transfer-matrix method is also applied to the dilatational mode in order to confirm the validity of our numerical scheme for the transmission rates.

A. Formulation

In applying the transfer-matrix method for a system with varying cross-sectional area, we first subdivide the wire into small segments in the longitudinal (x) direction so that each segment can be regarded to have a uniform cross-sectional area. This means that in each segment, we may solve the equations of motion (5), (10), (19), and (20) for obtaining the quantities needed in this scheme. Then, we apply appropriate boundary conditions (depending on the vibrational mode) at each interface of the segments as described below.

We represent the physical variables in the nth segment, which should be continuous at each interface, as a column vector $\mathbf{W}_n(x)$ and write this formally as

$$\mathbf{W}_n(x) = M_n(x)\mathbf{b}_n, \tag{33}$$

where $\mathbf{b}_n$ is a vector consisting of the amplitudes independent of the position x. Explicit expressions for $\mathbf{W}_n$ and M_n for each mode have been given in Appendix A. As we shall see below, for the dilatational and torsional modes the $\mathbf{b}_n$ vector consists of two components—i.e., $\mathbf{b}_n=(b_n^{(+)},b_n^{(-)})^t$, the amplitudes of the transmitted (propagating in the $+x$ direction) and reflected (propagating in the $-x$ direction) waves, respectively. For the coupled flexural-shear modes, however, $\mathbf{b}_n$ consists of four components corresponding to the transmitted and reflected components of the flexural (F) and shear (S) modes—i.e., $\mathbf{b}_n=(b_{F,n}^{(+)},b_{F,n}^{(-)},b_{S,n}^{(+)},b_{S,n}^{(-)})^t$. In accordance with these considerations, $M_n(x)$ is a 2×2 matrix for the dilatational and torsional modes and a 4×4 matrix for the flexural-shear modes.

Next, we introduce the transfer matrix F which connects the amplitude vector $\mathbf{b}_H=(b_H^{(+)},b_H^{(-)})^t$ in the lead adjacent to the hot reservoir to $\mathbf{b}_C=(b_C^{(+)},b_C^{(-)})^t$ in the lead adjacent to the cold reservoir as

$$\mathbf{b}_H = F\mathbf{b}_C. \tag{34}$$

With this matrix F the transmission rate of the vibrational energy through the wire is calculated. Explicitly, F is constructed in terms of the matrix $M_n(x)$ at each interface $x=x_n$ as

$$F = \prod_{n=0}^{N} H_n, \tag{35}$$

$$H_n \equiv [M_n(x_n)]^{-1}M_{n+1}(x_n), \tag{36}$$

where N is the total number of the segments in the wire, $x_0=-a$, and $x_N=a$ (the length of the wire is $2a$).

In the calculation of the transmission coefficient t_m, we can regard that only transmitted components are present in the lead attached to the cold reservoir—i.e., $b_C^{(-)}=0$. This leads to

$$t_m = (F_{11})^{-1} \tag{37}$$

for m, the dilatational ($m=D$) and torsional modes ($m=T$). The transmission rate is defined by the ratio of the incident and transmitted acoustic Poynting vectors and for these two modes it is simply given by $|t_m|^2$. In contrast, for the coupled flexural-shear modes the transmission coefficients should be discriminated according to the incident (m) and transmitted (m') modes and we denote them as $\tilde{t}_{mm'}$. Thus,

$$\tilde{t}_{FF} = \frac{F_{33}}{D}, \quad \tilde{t}_{FS} = -\frac{F_{31}}{D}, \tag{38}$$

if the incident mode is the flexural ($m=F$), and

$$\tilde{t}_{SS} = \frac{F_{11}}{D}, \quad \tilde{t}_{SF} = -\frac{F_{13}}{D}, \tag{39}$$

if the incident mode is the shear ($m=S$). In these expressions $D\equiv F_{11}F_{33}-F_{13}F_{31}$. Then, summing over the modes of the transmitted components coupled to the incident modes, the transmission rates $|t_m|^2$ of the flexural and shear modes are calculated as

$$|t_{m=F}|^2 = |\tilde{t}_{FF}|^2 + |\tilde{t}_{FS}|^2\frac{k_S}{k_F} \tag{40}$$

for the flexural mode and

$$|t_{m=S}|^2 = |\tilde{t}_{SS}|^2 + |\tilde{t}_{SF}|^2\frac{k_F}{k_S} \tag{41}$$

for the shear mode. It should be noted that for a given frequency the wave numbers k_F and k_S of the flexural and shear modes are determined by Eq. (21) as discussed in Sec. II C.

Here we note that for the flexural and shear modes that are coupled to each other, the transfer-matrix method for the transmission rates is stable only at low frequencies or for small wave numbers. This is because the shear vibrations of the wire that are excited above certain cutoff frequencies are evanescent modes below these frequencies. Hence, the associated vibrational amplitudes have exponentially growing components that become too large when the products of the transfer matrices are calculated. In this case we may use the more sophisticated scattering-matrix method as explained in Appendix B.

B. Analytic results for the dilatational mode

In order to check the validity of the numerical scheme based on the transfer-matrix method (and also the scattering-matrix method), we first apply it to the calculation of the transmission rate of the dilatational mode and compare with the analytical result.

The transmission rate $|t_{m=D}|^2$ of the dilatational mode through the catenoidal wire is obtained analytically and given by

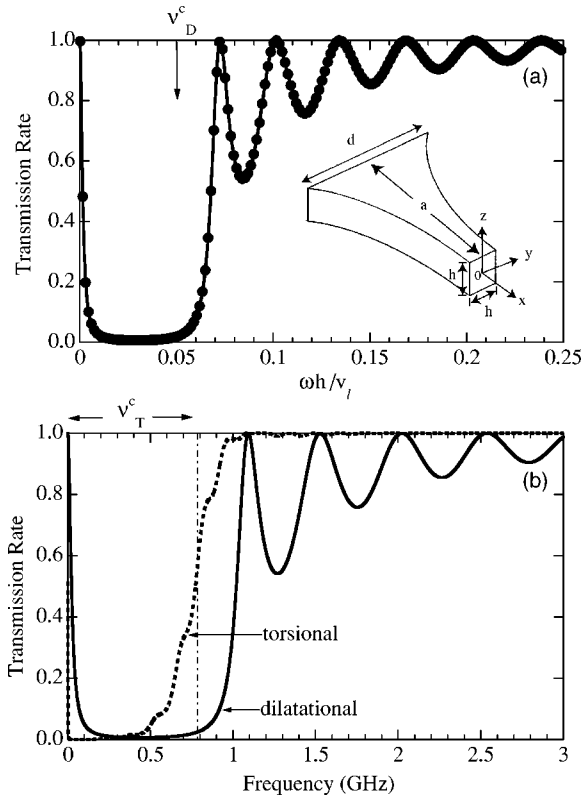

FIG. 2. (a) The transmission rate versus normalized frequency of the dilatational vibrations in a catenoidal GaAs wire. The solid line is the analytical result and dots are calculated with the transfer-matrix method. The parameters used are $\lambda=0.86$ μm, $d=2$ μm, and $h=0.05$ μm. ν_D^c is the cutoff frequency of the dilatational mode. The inset shows the definition of parameters characterizing the catenoidal wire (the only negative x region is shown). (b) The calculated transmission rates of the dilatational mode (solid line) and torsional mode (dotted line) in the same GaAs wire as for (a). ν_T^c denotes the cutoff frequencies of the torsional mode.

$$|t_{m=D}|^2 = 4K^2\left[\left(2Q\cos 2ka - \frac{Q^2-k^2-K^2}{k}\sin 2ka\right)^2 + 4K^2\left(\cos 2ka - \frac{Q}{k}\sin 2ka\right)^2\right]^{-1}, \tag{42}$$

for $\omega \geqslant \omega_D^c = v_l/\lambda$ and

$$|t_{m=D}|^2 = 4K^2\left[\left(2Q\cosh 2\kappa a - \frac{Q^2+\kappa^2-K^2}{\kappa}\sinh 2\kappa a\right)^2 + 4K^2\left(\cosh 2\kappa a - \frac{Q}{\kappa}\sinh 2\kappa a\right)^2\right]^{-1}, \tag{43}$$

for $\omega \leqslant \omega_D^c$. In these expressions

$$Q = \lambda^{-1}\tanh(a/\lambda), \tag{44}$$

$$\omega^2 = v_l^2K^2 = v_l^2[k^2 + (1/\lambda)^2] = v_l^2[-\kappa^2 + (1/\lambda)^2], \tag{45}$$

and $\kappa = ik$.

From Eqs. (42) and (43) the resonant transmissions [$|t_{m=D}|^2=1$ seen in Fig. 2(a)] are found to occur at frequencies ω satisfying

$$\frac{1}{k}\tan 2ka = \lambda\tanh\left(\frac{2a}{\lambda}\right) \tag{46}$$

for $\omega \geqslant \omega_D^c$ and

$$\frac{1}{\kappa}\tanh 2\kappa a = \lambda\tanh\left(\frac{2a}{\lambda}\right) \tag{47}$$

for $\omega \leqslant \omega_D^c$. At a frequency ω satisfying $\omega \ll \omega_D^c$ the transmission rate [Eq. (43)] is well described by the Lorentzian form

$$|t_{m=D}|^2 = \frac{1}{1+(\omega/\omega_0)^2}, \tag{48}$$

where $\omega_0^2 = v_l^2/(A^2+B)$ with

$$A = \frac{\lambda}{2}\left[\tanh\left(\frac{a}{\lambda}\right) + \sinh\left(\frac{2a}{\lambda}\right)\right] + \frac{a}{2}\left[1-\tanh^2\left(\frac{a}{\lambda}\right)\right], \tag{49}$$

$$B = -\left[\lambda a + \frac{\lambda^2}{2}\sinh\left(\frac{2a}{\lambda}\right)\right]\tanh\left(\frac{a}{\lambda}\right). \tag{50}$$

Evidently, $\omega=0$—i.e., $\kappa=\lambda^{-1}$—satisfies this resonance condition.

C. Numerical results of transmission rates

Based on the formulas developed above, we have numerically calculated the transmission rate for each mode of vibration through the catenoidal wire. The chosen parameters for the assumed GaAs wire are $\lambda=0.86$ μm and $h=50$ nm [the minimum cross-sectional area at the center of the wire is thus $A_0=A(x=0)=h^2=50\times 50$ nm^2], and the largest width at the ends of the wire is $d=2$ μm. Thus, the length of the wire is $2a=2\lambda\ln[\sqrt{d/h}+\sqrt{d/h-1}]=4.34$ μm. Also $Y=1.20\times10^{12}$ dyn cm^{-2} and $G=4.86\times10^{11}$ dyn cm^{-2} with $\rho=5.36$ g cm^{-3}, giving $v_l=4.73\times10^5$ cm s^{-1} and $v_t=3.01\times10^5$ cm s^{-1}.

Although the flexural-shear modes are coupled vibrations, we can conveniently regard them as separated flexural and shear modes as far as their transmission characteristics are concerned. It is only above a certain cutoff frequency $\omega=\omega_{S,min}$ defined below (numerically $\omega_{S,min}=30.4$ GHz with the above parameters) that these shear modes are excited effectively and their transmission probabilities become finite.

1. Dilatational mode

In order to check the validity of our numerical results, we show in Fig. 2(a) the analytically calculated transmission rate [Eqs. (42) and (43)] and the one calculated with the transfer-matrix method. In applying the transfer-matrix scheme, the number of divisions for the wire we have used are of the order of 10^3, for which the stability of the results has been confirmed. We see that the coincidence is excellent and thus we believe that our formulation for the transmission rates based on the transfer-matrix method (and also the scattering-matrix method for the coupled flexural and shear modes) is

quite convincing. Incidentally, the magnitude of the cutoff frequency $\omega_D^c \equiv v_l/\lambda$ for the dilatational mode is 0.88 GHz for the GaAs wire with $\lambda = 0.86$ μm.

2. Torsional mode

In Fig. 2(b) we see that the transmission rate of the torsional mode exhibits similar behavior as the dilatational mode; that is, a dip in transmission is seen below about 0.8 GHz. However, the cutoff of the transmission is not as sharp as the case of the dilatational mode. We have also repeated the same calculation with the scattering-matrix method and have checked the exact coincidence of the transmission rates obtained by these different two methods.

The presence of the cutoff frequency for this mode is expected by the presence of the term proportional to $\partial\theta/\partial x$ in Eq. (14), which induces the damping in transmission. However, the prefactor $[h^2 l(x) + l^3(x)]/4h^2[l(x) - 0.627h]$ on the right-hand side of Eq. (14) suggests that the cutoff frequency for this mode depends on the position of the segments in the wire assumed. According to the approximation developed in Sec. II B, the minimum cutoff frequency is given by putting $x_n = \lambda$ in the expression $\omega_T^c = 2v_t/\lambda \cosh^2(x_n/\lambda)$ and we have $\omega_{T,min}^c = 0.028$ GHz. If we extrapolate this expression up to the center of the wire, the maximum value of the cutoff frequency is roughly estimated to be $\omega_{T,max}^c = 0.79$ GHz. This range of frequencies between $\omega_{T,min}^c$ and $\omega_{T,max}^c$ is shown in Fig. 2(b). The cutoff of this mode is, thus, not as sharp as for the dilatational mode.

3. Flexural modes (thickness and width directions)

For the flexural vibrations in the thickness direction (z direction), the transmission rate does not show any clear structure and stays almost at unity down to about 0.05 GHz as seen in Fig. 3(a). This is because it is assumed that the thickness is uniform in the wire. The estimated cutoff frequency for this mode is $\omega_{F,z}^c = v_l h/2\sqrt{3}\lambda^2 = 0.015$ GHz [see Sec. II C].

In contrast, the width of the wire (in the y direction) changes according to $\propto \cosh^2(x/\lambda)$. Thus the transmission rate of the flexural vibrations in the width direction is strongly frequency dependent and exhibits rich structure at low frequencies where the transmission is suppressed both for the dilatational and torsional modes. The cutoff frequency estimated for this mode depends on the position of the segment $\omega_{F,y}^c = 9v_l h \cosh^2(x_n/\lambda)/2\sqrt{3}\lambda^2$ [see Sec. II C]. The largest value is 5.2 GHz and the lowest value is roughly 0.13 GHz. Within this frequency range indicated in Fig. 3(b) we see several resonant peaks in transmission but unfortunately no analytical formula for these resonance frequencies has so far been derived.

4. Shear mode (thickness direction)

The finite transmission of the shear modes starts at a frequency around $\omega_{S,min} = 30.4$ GHz. The frequency dependence of the transmission for the shear mode in the thickness direction is very simple. The sharp rise in transmission is due to the fact that the cutoff frequency of this mode is given by $\omega_{S,z}^c = (\kappa GA/\rho I)^{1/2} = (12\kappa G/\rho h^2)^{1/2} \equiv \omega_{S,min}$ with

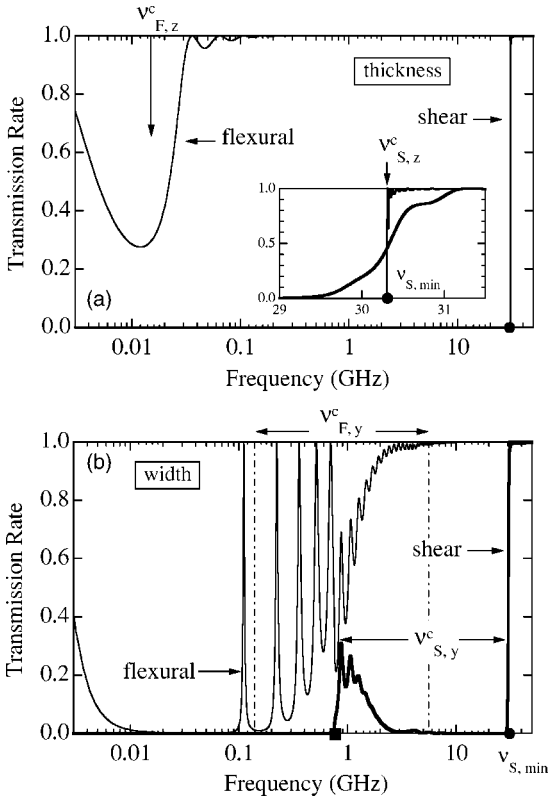

FIG. 3. The calculated transmission rates of the coupled flexural (thin line) and shear (bold line) mode (a) in the thickness direction and (b) in the width direction in the same GaAs wire as for Fig. 1. $\nu_{F,z}^c$ and $\nu_{F,y}^c$ ($\nu_{S,z}^c$ and $\nu_{S,y}^c$) are the cutoff frequencies of the flexural (shear) modes in the thickness and width directions, respectively. The inset of (a) shows the transmission rates in the frequency range where the shear mode rates become finite. The thin line (bold line) is the shear mode in the thickness direction (in the width direction). The rates of four acoustic modes are practically unity in this range. $\nu_{S,min}$ is the threshold frequency of the shear modes.

$I(x) = h^3 l(x)/12$. Thus, this value is independent of the position x of the wire and the shear mode is excited only for $\omega \geqslant \omega_{S,min}$ as shown in Fig. 3(a).

5. Shear mode (width direction)

For the shear mode in the width direction, however, $I(x) = hl(x)^3/12$ and the corresponding cutoff is $\omega_{S,y}^c = [12\kappa G/\rho l(x)^2]^{1/2} \propto l(x)^{-1}$. This means that the cutoff frequency $\omega_{S,y}^c$ depends again on the position in the wire and takes the maximum value equal to $\omega_{S,min}$ (dot in Fig. 3) at the center $x = 0$. The frequency $\omega_{S,y}^c$ becomes smaller as the position x of the wire shifts from the center and takes the minimum value $\omega_{S,min}/40 = 0.83$ GHz [solid square in Fig. 3(b)] at the both ends of the wire because $l(x = a)/h = d/h = 40$. Thus the transmission rate takes finite values at frequencies $\omega \geqslant \omega_{S,min}/40$ as shown in Fig. 3(b) and becomes unity at frequencies $\omega > \omega_{S,min}$ for which the shear mode is excited completely.

The behavior of the transmission rate in between $\omega_{S,min}/40$ and $\omega_{S,min}$ is understood as follows: For $\omega \simeq \omega_{S,min}/40$ the incident shear mode coming from the ideal

lead excites the shear mode only near the entrance of the wire but this mode cannot be transmitted through the center of the wire. The transmission is possible only via mode conversion into the flexural mode. This rate of the mode conversion should be large near the entrance where the shape of the wire changes rapidly. As the frequency increases the mode conversion into the flexural mode occurs near the center of the wire. However, the rate for this mode conversion to happen is small in the region where the width of the wire is almost uniform. We have numerically checked these characteristics of the mode conversion by changing the parameter λ determining the profile of the wire. At $\omega=\omega_{s,min}$ the mode conversion becomes irrelevant because the shear mode can be excited in the whole region of the wire. Accordingly, the gradual increase of the transmission rate seen for the shear vibrations in the width direction [inset of Fig. 3(a)] is qualitatively the same phenomenon as the one seen for the torsional mode.

IV. THERMAL CONDUCTANCE

With the transmission rates obtained in the preceding section, we have calculated the thermal conductance g for catenoidal wires of GaAs with various λ. An example for $\lambda=9.2$ μm is illustrated in Fig. 4(a). The contribution of each vibrational mode is shown in the inset. We see the presence of three plateaus in the temperature range $\sim 10^{-4}-1$ K. The plateau at $g/g_0=4$ ($T=0.02-0.2$ K) corresponds to the one studied theoretically by Rego and Kirczenow for GaAs wires[5] and also observed experimentally by Schwab *et al.* for silicon nitride wires.[3,4] Below this range of temperatures g/g_0 decreases from 4 because the overlapping of the phonon distribution function $\hbar\omega\partial n(\omega,T)/\partial T$ [Eq. (3)] with the dips in transmission for three acoustic modes except for the flexural vibration in the thickness direction becomes appreciable.

Another plateau at $g/g_0=6$ seen at higher temperatures is due to the excitation of shear modes of vibrations. Above about these temperatures additional optical modes of vibration with higher cutoff frequencies[15] would be excited and contribute to the heat conduction in the wire (we have not added the contribution of these modes). Hence, this plateau will be seen only when the higher optical phonon branches are well separated from the shear mode frequency $\omega_{S,min}$. Blencowe discussed that the broad nature of the Planckian distribution $n(\omega,T)$ should wash out the steps except for the one at the lowest temperature.[6] Thus the increase of g/g_0 from the plateau value 4 at a 1-K region is the indication of the onset of three-dimensional thermal conduction.

An interesting new observation is the recovery of g/g_0 seen at very low temperature after the breakdown of the quantization of $g/g_0=4$. In particular, an apparent plateau with nonintegral value of g/g_0 is seen for the wire with $\lambda=9.2$ μm below 1 mK. As we see in the inset of Fig. 4(a), this plateau appears as the temperature decreases due to the balance of the increasing and decreasing contributions of both the dilatational and flexural (in the width direction) modes to the conductance. At these temperatures (except for $T\rightarrow 0$) g/g_0 for the flexural mode in the thickness direction and the torsional mode stay unity and zero, respectively. The reason for the recovery of the quantized thermal conductance of the dilatational mode is the presence of the resonant transmission at $\omega=0$ [Eq. (48)].

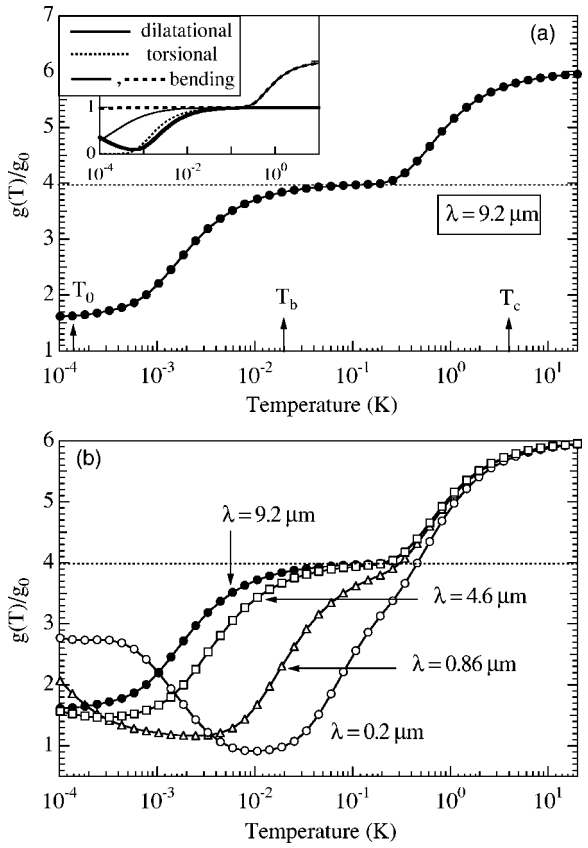

FIG. 4. (a) Calculated thermal conductance g (normalized by the quantum of thermal conductance $g_0=\pi^2k_B^2T/3h$) versus temperature for a GaAs catenoidal wire with $\lambda=9.2$ μm, $d=2$ μm, and $h=0.05$ μm. The inset shows the contributions of the dilatational mode (bold solid line), torsional mode (dotted line), and the coupled flexural-shear modes (denoted conveniently as bending modes) in the thickness direction (dashed line) and in the width direction (thin solid line). (b) g/g_0 for the catenoidal wires with various magnitude of λ—i.e., $\lambda=9.2$ μm (dots), $\lambda=4.6$ μm (squares), $\lambda=0.86$ μm (triangles), and $\lambda=0.2$ μm (open circles). The wire widths $d=2$ μm and $h=0.05$ μm are the same as (a). For T_0, T_b, and T_c indicated in (a), see the text.

Figure 4(b) further displays g/g_0 calculated for three other values of λ together with the one for $\lambda=9.2$ μm. The plateau region at $g/g_0=4$ is developed only for wires with large λ—that is, for the wires with a sufficiently large length in which the cross-sectional area is regarded to be uniform. No plateau at $g/g_0=4$ is recognizable at all for the wire with $\lambda=0.2$ μm. However, for this wire the presence of a dip in $g/g_0(\sim 1)$ is seen at temperatures for which the lower edge of the plateau $g/g_0=4$ exists for the wire with $\lambda=9.2$ μm. This normalized conductance then increases towards $g/g_0=4$ as the temperature decreases towards 0 K.

For comparison with the experimental observation of the plateau in g/g_0,[3,4] we have also carried out the calculation of the conductance for silicon nitride wires with the maximum and minimum widths 4 μm ($=d$) and 0.2 μm ($=\delta$), respec-

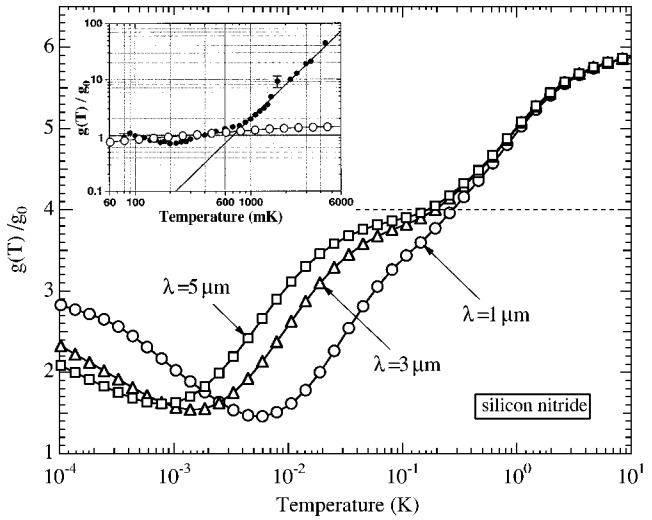

FIG. 5. Calculated thermal conductance g (normalized by the quantum of thermal conductance $g_0=\pi^2k_B^2T/3h$) versus temperature for catenoidal silicon nitride wires with $\lambda=1$ μm (circles), $\lambda=3$ μm (triangles), and $\lambda=5$ μm (squares). For other parameters of the wires, see the text. The inset shows the log-log plot which compares the experimental data by Schwab *et al.* (dots) with the theoretical results for $\lambda=1$ μm (circles).

tively, and with the uniform thickness 60 nm ($=h$).[17] The calculated temperature dependences are shown in Fig. 5. The effective wire length corresponding to the experiment by Schwab *et al.* is $2\lambda=2$ μm and the plateau is observed for 0.1–1 K as shown in the inset. However, for this value of λ the plateau does not develop in the calculated temperature dependence of g/g_0, but instead continues to decrease as the temperature goes down. (If we display the calculated g/g_0 in logarithmic scale rather than linear scale the coincidence with the experimental data is apparently good for the temperature range 0.1–1 K.) Theoretically, a reason is that the cutoff frequencies of the three of four acoustic modes except for the flexural vibration in the thickness direction are not fully separated from the onset frequency of the shear mode in the width direction $\omega^c_{S,\delta}=(12\kappa G/\rho\delta^2)^{1/2}=(12\kappa)^{1/2}v_t/\delta$. Numerically, $\omega^c_{S,\delta}=16.7$ GHz and $\omega^c_D=v_l/\lambda=1.60$ GHz, for instance. (Note that $\omega^c_{S,min}=30.4$ GHz and $\omega^c_D=0.88$ GHz for the GaAs wire with $\lambda=0.86$ μm.) This is also related to the fact that the minimum width $\delta=0.2$ μm at the center of the silicon nitride wire fabricated for the experiment is not small enough compared with the wire parameter $\lambda=1$ μm. This point will be also discussed in the next section.

V. DISCUSSION

In a catenoidal wire there exist three characteristic lengths h, λ, and a. Corresponding to the sizes of these lengths, we can define three characteristic temperatures. Two of them are readily defined with the relation $T=2\pi\hbar v/k_B\Lambda_{th}$ which connects the wavelength of dominant thermal phonons Λ_{th} and temperature T, where v is an appropriate sound velocity. (So these temperatures depend also on the vibrational mode.) Explicitly, $T=T_c\equiv 2\pi\hbar v/k_Bh$ and $T=T_b\equiv 2\pi\hbar v/k_B\lambda$ are obtained by putting $\Lambda_{th}=h$ and $\Lambda_{th}=\lambda$, respectively. The third characteristic temperature is defined by $T=T_0\equiv\hbar\omega_0/k_B=hv\exp(-2a/\lambda)/k_B\lambda$, where ω_0 is up to a numerical factor of the order of unity, equivalent to the one appearing in Eq. (48) for the dilatational mode if the condition $\exp(-2a/\lambda)\ll\exp(2a/\lambda)$ is satisfied.

Among these temperatures, T_c defines the temperature at which the crossover between the three- and one-dimensional thermal conductions occurs. For $T<T_c$, the wavelength of thermal phonons becomes longer than the width of the wire and the heat conduction is essentially that for the one-dimensional system. Thus, in this temperature region the quantization of g—i.e., the plateau in g/g_0—is expected to develop if the transmission of the relevant vibrational modes is perfect. This plateau only persists, however, as long as Λ_{th} is much shorter than the effective length of the wire—i.e., $\Lambda_{th}\ll\lambda$. Hence, the plateau may be well observed only under the condition $h\ll\Lambda_{th}\ll\lambda$ or $T_b\ll T\ll T_c$ in the temperature domain. At temperatures $T<T_b$ the plateau should be modified or, equivalently, the quantization breaks down in general. This clearly occurs as we can see in Fig. 4.

The last temperature T_0 gives a representative temperature at which the recovery of the quantization occurs. This is explicitly seen in the dilatational mode. The sharp rise in the transmission rate (up to unity) near $\omega=0$ (Fig. 2) is the resonance and the transmission rate is expressed by the Lorentzian form of Eq. (48) with the width ω_0. Similar but narrower transmission peaks at $\omega=0$ are also seen for other acoustic modes. Hence, at very low temperatures for which the phonon energy distribution $\hbar\omega\partial n(\omega,T)/\partial T$ is well confined inside this resonant peak in transmission—i.e., $T\ll T_0$—the quantization of the thermal conductance should be recovered. Actually, the recovering temperature of the quantization depends on the vibrational modes through their characteristic resonant transmission profiles near $\omega=0$. As we see in the inset of Fig. 4(a), the recovering temperature in the catenoidal wire is highest for the dilatational mode.

Numerically, those three temperatures for the dilatational mode are $T_c=4$ K, $T_b=0.02$ K, and $T_0=0.14$ mK, for $h=50$ nm, $\lambda=9.2$ μm, and $a=26.5$ μm ($d=2$ μm), and are indicated in Fig. 4(a). At $T=T_b$ and T_0 the expected transitions are clearly seen. In contrast, T_c is located below the temperature at which the plateau $g/g_0=6$ is attained. Here we note that apart from a numerical factor of the order of unity, T_c is essentially equal to the onset temperature $T_S=\hbar\omega_{S,min}/k_B=1.6$ K of the shear mode. Thus the excitation of the optical modes of vibrations and three-dimensional heat conduction is physically equivalent. This means that our analysis including only lowest two shear modes is not reliable for $T>T_c$. Blencowe has calculated the temperature dependence of g/g_0 in both sides of T_c for wires with uniform, rectangular cross sections. He found that there exists no steplike feature except for the plateau $g/g_0=4$ at $T\to 0$.[6] However, there still exists an expectation that the plateau at $g/g_0=6$ can be observed. This will happen if the wire is designed so that a gap of an appropriate magnitude may exist in between the lowest two shear mode branches we have considered and the next lowest optical branch in the wire. The vibrational frequencies in such wires can be studied with

a resonant ultrasound spectroscopy method by Visscher *et al.*, for example.[16]

Finally, we remark on the fact that the wires composed of softer materials are more appropriate to observe the quantization of thermal conductance. According to the discussion given above, the temperature range where the quantization of thermal conductance (or plateau) is expected to appear is $\Delta T = T_c - T_b$. Since both T_c and T_b are proportional to velocity v, the width of this range ΔT is also proportional to v and ΔT is smaller for softer materials. However, as we see in Fig. 4(a), the width of the plateau is actually smaller than ΔT because at $T = T_c$ optical modes are already excited; that is, the three-dimensional conduction has started at a temperature below T_c. This means that T_b (the lower edge of the plateau) is more important to observe the quantization effect. For softer materials with lower T_b the plateau in g/g_0 should be developed more extensively than that for harder materials. This is indeed recognized by comparing Fig. 4 (g/g_0 in GaAs wires) with Fig. 5 (g/g_0 in silicon nitride wires). For a softer GaAs wire with $\lambda = 4.6$ μm the plateau develops more clearly than that for a wire of harder silicon nitride with $\lambda = 5$ μm.

VI. CONCLUSIONS

In the present study we have investigated the thermal conductance in catenoidal wires of nanoscale dimensions by explicitly calculating the transmission rates of the low-lying six vibrational modes (four acoustic modes and two optical modes) that contribute to the heat transport at low temperatures. As far as the plateau (at $g/g_0 = 4$) associated with the universal quantized thermal conductance is concerned, three acoustic modes (other than the dilatational mode) not studied by Rego and Kirczenow contribute similarly to realize $g/g_0 = 4$ over an appreciable range of temperature, although the details are quite different depending on the mode. We have also considered how the quantization of the conductance changes in catenoidal wires as the temperature decreases further. The reduction and recovery of the conductance relative to the universal thermal quantum are predicted. They happen owing to the imperfect transmission of thermal energies due to the presence of cutoff frequencies for the acoustic vibrational modes in catenoidal wires and also the presence of resonances at zero frequency.

Our calculation indicates that the plateau at $g/g_0 = 4$ is not well developed for the silicon nitride wire (with $\lambda = 1$ μm) used in the experiment. The wire we assumed is symmetric with respect to $x = 0$ (the narrowest position) along the heat flow direction. We have also calculated the transmission rate of the dilatational mode by introducing some asymmetry as in the experimental phonon device by Schwab *et al.*[3,4] No large effect which may change the above result has been recognized. The plateau region is, however, predicted to become broader as the length of the wire becomes longer. So it would be interesting to measure the thermal conductance by changing the wire length. The theoretical search for the shape of quantum wires which allows the quantization of the thermal conductance for a wider range of temperatures would also be important.

ACKNOWLEDGMENTS

We thank M. Blencowe for helpful comments on the manuscript. This work was supported in part by the Grant-in-Aid for Scientific Research from the Ministry of Education, Science and Culture of Japan (Grant Nos. 09640385 and 16710097).

APPENDIX A

In this appendix we give explicit expressions for the vector $\mathbf{W}_n(x)$ and matrix M_n needed to define the transfer matrix for the calculation of the transmission rate of each vibrational mode.

1. Dilatational mode

For the dilatational mode $\mathbf{W}_n(x)$ is chosen as

$$\mathbf{W}_n(x) = \begin{pmatrix} u_n(x) \\ p_n(x) \end{pmatrix}, \tag{A1}$$

where p_n is the pressure in the nth segment and this pressure is obtained from the equation $p(x) = A(x)\sigma(x) = A(x)Y\partial u/\partial x$. The matrix M_n is

$$M_n = \begin{pmatrix} \exp(ik_n x) & \exp(-ik_n x) \\ ik_n Y A_n \exp(ik_n x) & -ik_n Y A_n \exp(-ik_n x) \end{pmatrix}, \tag{A2}$$

where $k_n = k = \omega/v_l$ and A_n are the wave number and the cross-sectional area in the nth segment, respectively.

2. Torsional mode

For the torsional mode $\mathbf{W}_n(x)$ is chosen as

$$\mathbf{W}_n(x) = \begin{pmatrix} \theta_n(x) \\ \tau_n(x) \end{pmatrix}, \tag{A3}$$

where $\tau(x)$ is the torque defined with the torsional rigidity C by $\tau(x) = C(x)\partial\theta/\partial x$. The matrix M_n is given by

$$M_n = \begin{pmatrix} \exp(ik_n x) & \exp(-ik_n x) \\ ik_n C_n \exp(ik_n x) & -ik_n C_n \exp(-ik_n x) \end{pmatrix}, \tag{A4}$$

where $k_n = (C_n/\rho\tilde{I}_n)^{-1/2}\omega$ and $\tilde{I}$ is the polar moment of inertia [Eq. (11)] in the nth segment.

3. Flexural-shear mode

For the flexural-shear mode $\mathbf{W}_n(x)$ is a four-component vector—i.e.,

$$\mathbf{W}_n(x) = \begin{pmatrix} w_n(x) \\ S_n(x) \\ \psi_n(x) \\ \mu_n(x) \end{pmatrix}, \tag{A5}$$

where $S(x)$ is the shear stress defined by $S(x) = \kappa GA(x)[\partial w/\partial x - \psi(x)]$ and $\mu(x)$ is the bending moment defined by $\mu(x) = YI(x)\partial\psi/\partial x$. The matrix M_n is given by

$$M_n(x) = \begin{pmatrix} M_{1j}(x) \\ M_{2j}(x) \\ M_{3j}(x) \\ M_{4j}(x) \end{pmatrix} = \begin{pmatrix} \exp(ik_n^{(j)}x) \\ G\kappa A_n(ik_n^{(j)} - \phi_n^{(j)})\exp(ik_n^{(j)}x) \\ \phi_n^{(j)} \exp(ik_n^{(j)}x) \\ ik_n^{(j)} Y I_n \exp(ik_n^{(j)}x) \end{pmatrix}$$

$$(j = 1 - 4),$$

where ϕ is the ratio between ψ and w, and $k^{(j)}$ are given by the solutions of Eq. (21) (for a given ω) with I_0 and A_0 replaced by I_n and A_n.

APPENDIX B: SCATTERING MATRIX METHOD

The transfer matrix connects the waves in one end to the other end of the system. So, if there exist waves which vary exponentially with distance, the numerical scheme with the transfer-matrix method becomes unstable, in general. In order to avoid this numerical instability we can use the scattering matrix ($\tilde{F}$) which connects the amplitude vector $\mathbf{b}_{in}$ associated with the incoming waves in the leads attached to the hot (H) and cold (C) reservoirs to the one $\mathbf{b}_{out}$ for the outgoing waves in the leads—i.e., $\mathbf{b}_{out} = \tilde{F}\mathbf{b}_{in}$, where $\mathbf{b}_{out} = (b_C^{(+)}, b_H^{(-)})^t$ and $\mathbf{b}_{in} = (b_H^{(+)}, b_C^{(-)})^t$ for the longitudinal or torsional mode and $\mathbf{b}_{out} = (b_{F,C}^{(+)}, b_{S,C}^{(+)}, b_{F,H}^{(-)}, b_{S,H}^{(-)})^t$ and $\mathbf{b}_{in} = (b_{F,H}^{(+)}, b_{S,H}^{(+)}, b_{F,C}^{(-)}, b_{S,C}^{(-)})^t$ for the flexural and shear modes. (The notations are the same as for the transfer-matrix method developed in Sec. III A.) In the calculation of the transmission coefficient t_m, we can assume that only transmitted components exist in the lead attached to the cold reservoir (e.g., $b_C^{(-)} = 0$). Thus, we can get $t_m = \tilde{F}_{11} = b_C^{(+)}/b_H^{(+)}$ for m, the dilatational and torsional modes. For the coupled flexural-shear modes the transmission coefficients are given by

$$t_{FF} = b_{F,C}^{(+)}/b_{F,H}^{(+)} = \tilde{F}_{11}, \quad t_{FS} = b_{S,C}^{(+)}/b_{F,H}^{(+)} = \tilde{F}_{21} \tag{B1}$$

if the incident mode is flexural ($b_{S,H}^{(+)} = 0$) and

$$t_{SF} = b_{F,C}^{(+)}/b_{S,H}^{(+)} = \tilde{F}_{12}, \quad t_{SS} = b_{S,C}^{(+)}/b_{S,H}^{(+)} = \tilde{F}_{22} \tag{B2}$$

if the incident mode is shear ($b_{F,H}^{(+)} = 0$).

The procedure for obtaining the scattering matrix is the following. (Though we here consider the scattering matrix composed of a 2×2 matrix, the generalization to a $m \times m$ matrix is straightforward.) First we write the matrix H_n in Eq. (36) as

$$H_n = \begin{pmatrix} h_{11}^{(n)} & h_{12}^{(n)} \\ h_{21}^{(n)} & h_{22}^{(n)} \end{pmatrix}.$$

Next we introduce the matrix

$$s_n = \begin{pmatrix} s_{11}^{(n)} & s_{12}^{(n)} \\ s_{21}^{(n)} & s_{22}^{(n)} \end{pmatrix}$$

at each interface $x = x_n$, which is defined by

$$\begin{pmatrix} b_{n+1}^{(+)} \\ b_n^{(-)} \end{pmatrix} = \begin{pmatrix} s_{11}^{(n)} & s_{12}^{(n)} \\ s_{21}^{(n)} & s_{22}^{(n)} \end{pmatrix} \begin{pmatrix} b_n^{(+)} \\ b_{n+1}^{(-)} \end{pmatrix}. \tag{B3}$$

With the elements of H_n, the matrix s_n is represented by

$$s_n = \begin{pmatrix} h_{11}^{(n)} - h_{12}^{(n)}[h_{22}^{(n)}]^{-1}h_{21}^{(n)} & h_{12}^{(n)}[h_{22}^{(n)}]^{-1} \\ [h_{22}^{(n)}]^{-1}h_{21}^{(n)} & [h_{22}^{(n)}]^{-1} \end{pmatrix}. \tag{B4}$$

Hence, it is convenient to define the combination law which constructs the matrix S in terms of s_n and s_{n+1} as $S = s_{n+1} \otimes s_n$—i.e.,

$$\begin{pmatrix} b_{n+2}^{(+)} \\ b_n^{(-)} \end{pmatrix} = \begin{pmatrix} S_{11} & S_{12} \\ S_{21} & S_{22} \end{pmatrix} \begin{pmatrix} b_n^{(+)} \\ b_{n+2}^{(-)} \end{pmatrix}. \tag{B5}$$

In this combination law the matrix elements of S are given by

$$S_{11} = [s_{n+1} \otimes s_n]_{11} = s_{11}^{(n+1)}[1 - s_{12}^{(n)}s_{21}^{(n+1)}]^{-1}s_{11}^{(n)}, \tag{B6}$$

$$S_{12} = [s_{n+1} \otimes s_n]_{12} = s_{12}^{(n+1)} + s_{11}^{(n+1)}[1 - s_{12}^{(n)}s_{21}^{(n+1)}]^{-1}s_{12}^{(n)}s_{22}^{(n+1)}, \tag{B7}$$

$$S_{21} = [s_{n+1} \otimes s_n]_{21} = s_{21}^{(n)} + s_{22}^{(n)}[1 - s_{21}^{(n+1)}s_{12}^{(n)}]^{-1}s_{21}^{(n+1)}s_{11}^{(n)}, \tag{B8}$$

$$S_{22} = [s_{n+1} \otimes s_n]_{22} = s_{22}^{(n)}[1 - s_{21}^{(n+1)}s_{12}^{(n)}]^{-1}s_{22}^{(n+1)}. \tag{B9}$$

Using the above procedures recursively, we can obtain the scattering matrix $\tilde{F}$, which is given by

$$\tilde{F} = [[[s_0 \otimes s_1] \otimes s_2] \otimes \cdots] \otimes s_N. \tag{B10}$$

Thus, in the scattering-matrix method, the relevant matrix elements correspond to the transmission or reflection coefficients at each recursive stage [Eqs. (B1) and (B2)] and there is no numerical instability even if waves with exponentially increasing and/or decreasing components arise.[14]

[1] For a recent review, see M. P. Blencowe, Phys. Rep. **395**, 159 (2004).

[2] A. N. Cleland, *Foundations of Nanomechanics* (Springer, Berlin, 2003).

[3] K. Schwab, E. A. Henriksen, J. M. Worlock, and M. L. Roukes, Nature (London) **404**, 974 (2000).

[4] K. Schwab, J. L. Arlett, J. M. Worlock, and M. L. Roukes, Physica E (Amsterdam) **9**, 60 (2001).

[5] L. G. C. Rego and G. Kirczenow, Phys. Rev. Lett. **81**, 232 (1998).

[6] M. P. Blencowe, Phys. Rev. B **59**, 4992 (1999).

[7] See, also, D. E. Angelescu, M. C. Cross, and M. L. Roukes, Superlattices Microstruct. **23**, 673 (1998).

[8] R. Landauer, IBM J. Res. Dev. **1**, 223 (1957).

[9] U. Sivan and Y. Imry, Phys. Rev. B **33**, 551 (1986).

[10] D. H. Santamore and M. C. Cross, Phys. Rev. B **66**, 144302

(2002).
[11] S. P. Timoshenko and J. N. Goodier, *Theory of Elasticity* (McGraw-Hill, New York, 1970).
[12] K. F. Graff, *Wave Motion in Elastic Solids* (Dover, New York, 1975).
[13] P. M. Morse, *Vibration and Sound* (McGraw-Hill, New York, 1936).
[14] See, for instance, David Yuk Kei Ko and J. C. Inkson, Phys. Rev. B **38**, 9945 (1988); L. Li, J. Opt. Soc. Am. A **13**, 1024 (1996).
[15] N. Nishiguchi, Y. Ando, and M. N. Wybourne, J. Phys.: Condens. Matter **9**, 5751 (1997).
[16] W. M. Visscher, A. Migliori, T. M. Bell, and R. A. Reinert, J. Acoust. Soc. Am. **90**, 2154 (1991).
[17] For a glassy silicon nitride wire we employ the isotropic approximation to estimate the elastic properties. This leads to $Y=3.24\times10^{12}$ dyn cm^{-2} and $G=1.33\times10^{12}$ dyn cm^{-2}, and with $\rho=3.20$ g cm^{-5} we obtain $v_l=10.07\times10^5$ cm s^{-1} and $v_t=6.45\times10^5$ cm s^{-1}. For the original data of the elastic constants for crystalline Si_3N_4, see R. Vogelgesang, M. Grimsditch, and J. S. Wallace, Appl. Phys. Lett. **76**, 982 (2000).